Journal of Magnetism and Magnetic Materials 594 (2024) 171906

Contents lists available at ScienceDirect

Journal of Magnetism and Magnetic Materials

journal homepage: www.elsevier.com/locate/jmmm

Research article

Quantum $SU(3)$-ferrimagnet on triangular lattice

A.S. Martynov, D.M. Dzebisashvili *

Kirensky Institute of Physics, Federal Research Center KSC SB RAS, 660036, Krasnoyarsk, Russia

ARTICLE INFO

Keywords:
Quantum $SU(3)$-ferrimagnet
Single-ion anisotropy
Quadrupole ordering
Triangular lattice

ABSTRACT

Manifestations of quantum effects in the macroscopic properties of frustrated magnets keep attracting considerable interest. We have formulated and studied a simple model of a three-sublattice mixed-spin ($S = 1, 1/2, 1/2$) $SU(3)$-ferrimagnet on triangular lattice in which the strong quantum fluctuations are developed due to combined effect of frustrated exchange bonds, reduced dimensionality and a single-ion easy-plane anisotropy in the spin-1 sublattice. To account correctly for the $SU(3)$ algebra, the Hubbard operators representation of generators is used. Dependencies of the magnetic moments R and R_L (for spin-1/2 and spin-1 sublattices respectively), the total magnetic moment M, as well as the quadrupole moment, on the anisotropy parameter D are calculated at zero temperature and different ratios I/J of exchange integrals from different sublattices. It is established that for $I/J \ll 1$ the critical value D_c, at which the system enters the quadrupole antiferromagnetic phase, can be much smaller than both I and J. Besides, with an increase in D from zero to D_c the total moment $\mathbf{M}$ can change its direction several times via taking zero value. Classification of four branches of the spin-wave excitation spectrum of the $SU(3)$-ferrimagnet is carried out and modification of the spectrum with change in the single-ion anisotropy is analyzed.

1. Introduction

Physical properties of ferrimagnets are often described within the phenomenological approach based on thermodynamic potential expansion and subsequent use of the Landau-Lifshitz equation [1]. Such an approach is justified if relativistic effects are insignificant. The quantum consideration of such ferrimagnets is based on the spin Hamiltonians with operators obeying $SU(2)$ algebra.

In last decades, magnetic materials have been actively studied, in which relativistic (viz. spin–orbit) interactions lead to manifestation of quantum effects at the macroscopic level [2–13]. Such materials are commonly referred to as quantum magnets [14]. Quantum effects are enhanced in systems of reduced dimension [15], as well as in the materials with frustrated bonds [16].

The simplest type of interaction making a magnet to be quantum appears due to taking into account the crystal field. If the energy of such an interaction, for instance, the energy of single-ion anisotropy (SIA), is not small, then to describe correctly the properties of a magnet, it is necessary to consider not only dipole degrees of freedom, but rather quadrupole ones [7,11,12,17–20].

The possibility of quadrupole ordering in $S = 1$ Heisenberg models was initially associated with additional biquadratic spin exchange interactions $(\mathbf{S}_i \cdot \mathbf{S}_j)^2$ with nearest sites i and j [21]. Later, Andreev and Grishchuk mentioned that the notion of quadrupoles can also be extended to $S = 1/2$ spins, albeit not with on-site, but rather with bond-based order parameters [6]. For larger spin values S the biquadratic Heisenberg models can be extended to account for bicubic exchange terms $(\mathbf{S}_i \cdot \mathbf{S}_j)^3$ [22] and further up to polynomial spin-S exchange interactions of order $2S$ [23]. All these extensions of the Heisenberg model lead to a quadrupole ordering in a certain parameter domain. Also, it should be noted that the so-called three-site interaction of the form $(\mathbf{S}_i \cdot \mathbf{S}_j)(\mathbf{S}_j \cdot \mathbf{S}_k)$ (which can be thought of as partly destroyed biquadratic interaction) was shown to be able to give a small admixture of quadrupolar component to the main chiral magnetic order [24]. Probably, the most advanced generalization of the quantum Heisenberg model is known as $SU(N)$-symmetric antiferromagnetic spin model [25–29] in which all generators of the $SU(N)$-group (all equally and pairwise symmetrically) are used instead of generators of the rotation group, i.e. spin operators. As a matter of fact, we believe, that accounting for any kind of (strong enough) interaction involving generators of $SU(N)$-algebra that are beyond the usual spin operators (such, for instance, as any degree of a spin operator) can be considered as sufficient to designate such an (anti)ferromagnet as $SU(N)$-(anti)ferromagnet.

In multi-sublattice ferrimagnets with different magnetic ions, manifestation of quantum effects can be significantly enhanced due to possible compensation of the effective field acting on the magnetoactive ions. Indeed, as was shown in [18] in the two-sublattice ferrimagnet,

* Corresponding author.
E-mail addresses: zldgin2@mail.ru (A.S. Martynov), ddm@iph.krasn.ru (D.M. Dzebisashvili).

https://doi.org/10.1016/j.jmmm.2024.171906
Received 10 January 2024; Received in revised form 16 February 2024; Accepted 26 February 2024
Available online 29 February 2024

the quantum spin reduction (i.e. a decrease in the sublattice average magnetization) in an anisotropic sublattice at low temperatures can be essentially reduced by the action of exchange interaction field of the isotropic sublattice. If there are more than two sublattices, then the effective field of two isotropic, antiferromagnetically coupled sublattices, acting on the ions of the third anisotropic sublattice, can turn to zero eliminating thereby the mentioned mechanism of suppression of quantum spin reduction.

Examples of such magnetic systems, which have been of great interest for quite a long time, are frustrated mixed spin-1/2 and spin-1 Ising ferrimagnets with SIA on square lattice [30–38] and recently on triangular lattice [39–41]. The main focus were their phase diagrams as well as technologically interesting compensation behavior with possibility to achieve zero total magnetization by tuning temperature below the critical point.

In these systems, the SIA in the spin-1 sublattice is an important source of zero-point quantum vibrations which, in particular, results in significant quantum spin reduction at zero temperature [3,5–9,11,42]. When parameter of the SIA is comparable to the value of exchange integrals, the magnetization complete suppression can occur. To describe this effect, the theory of strongly anisotropic magnet with SIA being developed should involve operators from $SU(3)$ algebra. Also, these systems are interesting from a perspective of both reduced (2d) dimensionality amplifying fluctuations, and geometric frustration in the case of triangular lattice [39–41].

In the present study we consider a three-sublattice mixed spin ferrimagnet on triangular lattice with taking into account the easy-plane SIA. In one sublattice, the spin value is taken to be $S = 1$ and in the other two sublattices $S = 1/2$. An important distinction of our model from that of Refs. [39–41] (based on the Ising model) is the use of the full Heisenberg exchange interaction which is known to enhance quantum fluctuations even more. In the case of square lattice a similar generalization of the anisotropic mixed-spin $S = (1/2, 1)$ ferrimagnets [30–38] with replacement of the Ising exchange with the Heisenberg one was performed in Ref. [43]. The significance of the three-sublattice mixed-spin anisotropic ferrimagnet to be considered in our study is due to the fact that it includes the combination of SIA, reduced dimension, geometric frustration as well as developed quantum fluctuations. Also, the emphasis is made not on the study of finite temperature behavior but rather on zero temperature properties inaccessible by Monte-Carlo simulations used in Refs. [39–41]. We focus mainly on the dependence of the ground state magnetic structure and energy spectrum on the single-ion anisotropy parameter at different ratios of exchange integrals. In what follows, for brevity and also taking into account the above, we refer the magnetic system under consideration as $SU(3)$-ferrimagnet (SU3-F).

The further presentation is organized as follows. In the second section, the Hamiltonian of the SU3-F is formulated. In Section 3, the $SU(2)$ transformation describing local coordinate axes rotation in two sublattices with spin-1/2 is applied to the Hamiltonian of SU3-F. In Section 4, using proposed in [8] variational function for spin-1 with easy-plane SIA, we analyzed the ground state properties of the system in the mean field approximation, and introduced the dipole and quadrupole order parameters. The Holstein-Primakov transformations for two sublattices with spin-1/2 are carried out in Section 5. In Section 6, the $SU(3)$ transformation in the Hubbard operators representation is used to diagonalize the single-site Hamiltonian of the spin-1 sublattice. To calculate spectral properties, the bosonization of Hubbard operators is performed in Section 7 and corresponding dispersion equation is presented in Section 8. The results of the ground state structure calculations and analysis of the spectral properties are presented in Sections 9 and 10, respectively. The main conclusions of the study are formulated in the Section 11.

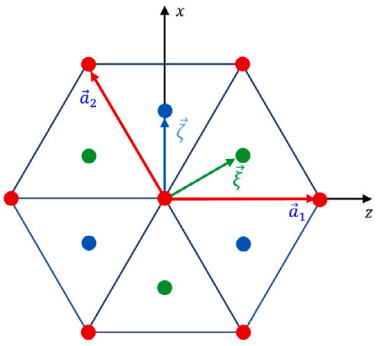

Fig. 1. Three triangular sublattices: L-sublattice with spin $S = 1$ (red), F- and G-sublattices with spin $S = 1/2$ (green and blue, respectively). Here $|\mathbf{a}_1| = |\mathbf{a}_2| = a$ are basis vectors, and the vectors ξ and ζ connect sites from different sublattices.

2. The model of $SU(3)$-ferrimagnet

The crystalline structure of the three-sublattice anisotropic $SU(3)$-ferrimagnet on triangular lattice is shown in Fig. 1. Here, the sites hosting spins $S = 1$ are highlighted in red. These sites form sublattice denoted further by the symbol L. The green and blue sites contain spins $S = 1/2$. The sublattices formed by these sites are denoted as F- and G-sublattices, respectively. Periodicity of each sublattice is determined by the basis vectors $\mathbf{a}_1$ and $\mathbf{a}_2$, and the vectors ξ and ζ connect sites from different sublattices.

The Hamiltonian of the three-lattice SU3-F under consideration has the form:

$$H = H_A + H_{exch}, \tag{1}$$

where

$$H_A = D \sum_l \left(S_l^y\right)^2,$$

$$H_{exch} = J \sum_{\{fg\}} \mathbf{S}_f \cdot \mathbf{S}_g + I \sum_{\{fl\}} \mathbf{S}_f \cdot \mathbf{S}_l + I \sum_{\{gl\}} \mathbf{S}_g \cdot \mathbf{S}_l. \tag{2}$$

In the expression (1), the operator H_A takes into account the energy of SIA in L-sublattice with spin $S = 1$ and with anisotropy constant D being positive. The site indices from this L-sublattice are below denoted by l, and corresponding spin projection operators by S_l^α ($\alpha = x, y, z$). The axis Oy is directed perpendicular to the plane of the ferrimagnet. Accordingly, the axes Ox and Oz define its plane. The site indices for other two F- and G-sublattices with $S = 1/2$ are indicated by f and g, and the vector spin operators by $\mathbf{S}_f$ and $\mathbf{S}_g$, respectively. The energy operator H_{exch} describes the exchange interaction between a spin-1 subsystem and two spin-1/2 subsystems, as well as the exchange interaction between two spin-1/2 subsystems. The intensity of these antiferromagnetic interactions is determined by integrals I and J, respectively. Curly brackets under the three sum symbols in (2) mean that the summation is carried out only over the nearest sites and each pair of sites is counted only once.

3. $SU(2)$ transformation of the Hamiltonian

For different sublattices the Lande g-factors are different and the existence, for instance, of a compensation point for the total mechanical moment does not mean that the total magnetic moment is also equal to zero at this point [43]. However in what follows we will assume that all moments have the same, purely spin (not orbital) nature, and therefore g-factors in all sublattices are equal to each other ($g = 2$). This allows to omit for simplicity the multiplier $g\mu_B$ in the equation $\mathbf{R} = -g\mu_B\langle\mathbf{S}\rangle$, relating magnetic $\mathbf{R}$ and spin $\langle\mathbf{S}\rangle$ moments, and to determine the equilibrium magnetization vectors in each sublattice in the units of $g\mu_B$ as $\mathbf{R}_A = \langle\mathbf{S}_A\rangle$ ($A = L, F$ and G), bearing of course in

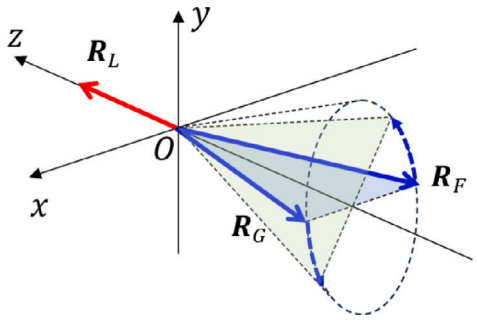

Fig. 2. Planar magnetic structure of the SU3-F. All spins lie in the zOx plane which is the easy-plane. Rotation of the plane of vectors $\mathbf{R}_F$ and $\mathbf{R}_G$ is supposedly unfavorable due to indirect effect of the SIA on the spins in the F- and G-sublattices (see discussion in the main text).

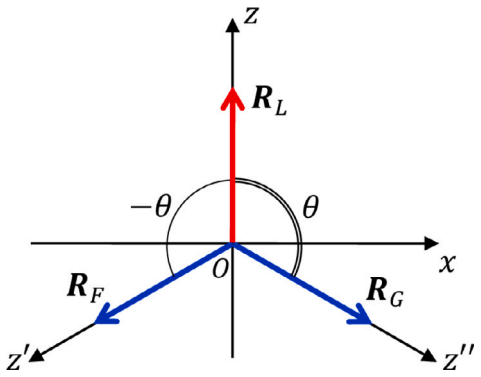

Fig. 3. Rotation of local coordinate axes under unitary transformation (3). In F- and G-sublattices with $S = 1/2$, the Oz-axes are rotated at the angles $-\theta$ and θ and take new positions Oz' and Oz'' along equilibrium sublattice magnetizations $\mathbf{R}_F$ and $\mathbf{R}_G$, respectively. The Oz axis in the L-sublattice with $S = 1$ is invariant under the transformation (3).

mind that, due to the minus sign, the true direction of magnetization is the opposite. The latter circumstance is not essential in the absence of magnetic field.

The easy-plane anisotropy suggests that the magnetization vector $\mathbf{R}_L$ of L-sublattice lies in the zOx plane (i.e. perpendicular to the anisotropy axis Oy). We choose the direction of the Oz-axis along the vector $\mathbf{R}_L$ (Fig. 2). At the same time, due to antiferromagnetic exchange interaction between the spins of all three sublattices, the magnetic structure must be planar. It is seen that, at least at the mean-field level, the energy of the SU3-F is invariant with respect to rotation of the plane of vectors $\mathbf{R}_F$ and $\mathbf{R}_G$ around Oz-axis as is shown in Fig. 2. It means that the vectors $\mathbf{R}_F$ and $\mathbf{R}_G$ do not necessarily have to lie in the zOx-plane. Nevertheless, our assumption is that spins in the F- and G-sublattices can feel the SIA indirectly, via the L-subsystem, in higher orders of perturbation theory, and this "feeling" will compel the vectors $\mathbf{R}_F$ and $\mathbf{R}_G$ to lie in the zOx-plane. We however will not be concerned with the higher-order corrections in the present study and will consider the chosen orientation of the vectors $\mathbf{R}_F$ and $\mathbf{R}_G$ as spontaneous breaking of rotational symmetry. This point will be essential when discussing spectral properties of the SU3-F in Section 10.

In order to study the ground state and energy spectrum of the SU3-F, we, first of all, carry out $SU(2)$-transformation of the Hamiltonian, which is well known in the theory of non-collinear antiferromagnets and which corresponds to a change in local coordinate axes. In our case, this is achieved by rotating the original coordinate system by an angle of $\theta(-\theta)$ around the Oy axis for ions from G-(F-) sublattice in such a way that the new axis $Oz''(Oz')$ is oriented along the vector of equilibrium magnetization $\mathbf{R}_G(\mathbf{R}_F)$ as is shown in Fig. 3. The aforesaid means performing the following $SU(2)$-transformation of the Hamiltonian

$$H \to H(\theta) = U_2(\theta)\, H\, U_2^{\dagger}(\theta) \tag{3}$$

where the unitary operator is

$$U_2(\theta) = \prod_{f\in F} \exp\left(-i\theta S_f^y\right) \prod_{g\in G} \exp\left(i\theta S_g^y\right). \tag{4}$$

The operator $H(\theta)$ can be written explicitly using the transformation laws for spin operators (see Appendix A):

$$S_g^x \to S_g^x \cos\theta + S_g^z \sin\theta, \quad S_g^y \to S_g^y,$$
$$S_g^z \to S_g^z \cos\theta - S_g^x \sin\theta, \tag{5}$$

$$S_f^x \to S_f^x \cos\theta - S_f^z \sin\theta, \quad S_f^y \to S_f^y,$$
$$S_f^z \to S_f^z \cos\theta + S_f^x \sin\theta. \tag{6}$$

As a result we get:

$$\begin{aligned} H_{exch}(\theta) = {} & J \sum_{\{fg\}} \Big[\sin 2\theta \left(S_f^x S_g^z - S_f^z S_g^x\right) \\ & + S_f^y S_g^y + \cos 2\theta \left(S_f^x S_g^x + S_f^z S_g^z\right)\Big] \\ & + I \sum_{\{fl\}} \Big[\sin\theta \left(S_f^x S_l^z - S_f^z S_l^x\right) + S_f^y S_l^y \\ & + \cos\theta \left(S_f^x S_l^x + S_f^z S_l^z\right)\Big] \\ & + I \sum_{\{gl\}} \Big[\sin\theta \left(S_g^z S_l^x - S_g^x S_l^z\right) + S_g^y S_l^y \\ & + \cos\theta \left(S_g^x S_l^x + S_g^z S_l^z\right)\Big]. \end{aligned} \tag{7}$$

The anisotropy energy operator remains unchanged $H_A(\theta) = H_A$.

4. Ground state of the $SU(3)$ ferrimagnet

The operator H_A, being quadratic in spin variables, describes quadrupole field effects. Accordingly, H_A initiates participation of quadrupole degrees of freedom in the formation of static and dynamic properties the SU3-F. For one- and two-sublattice magnetic systems manifestation of quantum effects due to H_A has been discussed in many papers [2,3,7,8,11,12]. In this section, we qualitatively, on the mean-field level, consider impact of quantum effects on the ground state structure of the three-sublattice anisotropic SU3-F.

First of all, we note that according to the Ref. [8], in the presence of SIA accounted by the operator H_A, the ground state of the magnetic ion in the L-sublattice should be looked for in the form

$$|\psi\rangle = \cos\alpha\, |+1\rangle + \sin\alpha\, |-1\rangle, \tag{8}$$

where ket-vectors in the right hand side are eigenstates of the spin-1 operator S_l^z on the l-site ($S_l^z|n\rangle = n|n\rangle$, $n = -1, 0, +1$) and α is a variational parameter. Note, that due to a not-small SIA the state $|0\rangle$ drops out of the variational function $|\psi\rangle$ [8]. Then, taking into account (7), for the energy of SU3-F per unit cell in the mean field approximation, we obtain

$$\begin{aligned} E(\theta,\alpha) = {} & J_0 S^2 \cos 2\theta + 2I_0 S \cos\theta \cos 2\alpha \\ & + D\,(1 - \sin 2\alpha)\,/2, \end{aligned} \tag{9}$$

where $J_0 = 3J$, $I_0 = 3I$ and $S = 1/2$. In the expression (9), the first two terms describe contributions of the exchange interaction of spins from different sublattices, and the last term is due to SIA. When writing (9), it was also taken into account that the equilibrium mean-field value of the L-sublattice magnetization is

$$R_L^{MF} = \langle\psi|S_l^z|\psi\rangle = \cos 2\alpha. \tag{10}$$

This value may differ significantly from the nominal one due to quantum effects.

It is essential that the average value of the quadrupole moment operator [44]

$$\hat{Q}_{yy} = 3\left(S_l^y\right)^2 - 2 \tag{11}$$

in the state (8)

$$Q^{MF} = \langle\psi|\hat{Q}_{yy}|\psi\rangle = 3(1-\sin 2\alpha)/2 - 2 \tag{12}$$

depends on the α parameter. This means that in SU3-F the quadrupole moment becomes an additional (relative to the spin) degree of freedom affecting both the static properties of the system and its dynamic characteristics.

At $I, J > 0$ in the isotropic limit ($D = 0$) it follows from the expression (9) that:

$$\begin{aligned} &\alpha = 0, \quad \theta = \pi, \quad \text{if} \quad I_0 \geqslant 2J_0 S, \\ &\alpha = 0, \quad \cos\theta = -\frac{I_0}{2J_0 S}, \quad \text{if} \quad I_0 \leqslant 2J_0 S. \end{aligned} \tag{13}$$

For $D > 0$, there is a critical value

$$D_c = 2I_0^2/J_0 \tag{14}$$

such that for $D < D_c$ the equilibrium values of the parameters α and θ are determined by the expressions

$$\begin{aligned} &\sin 2\alpha = D/D_c, \quad \cos\theta = -(I_0/2J_0 S)\cdot R_L^{MF}, \\ &R_L^{MF} = \sqrt{1-(D/D_c)^2}. \end{aligned} \tag{15}$$

If $D > D_c$, then

$$\alpha = \pi/4, \quad \theta = \pi/2, \quad R_L = 0. \tag{16}$$

Such a solution corresponds to a configuration in which the spins in the F- and G-sublattices are ordered antiferromagnetically with respect to each other, whereas the ions in the L-sublattice are in a "non-magnetic" state, but with $Q^{MF} = -2$, i.e. in a quadrupole antiferromagnetic phase (QAFM).

It is important to note that quantum effects in SU3-F can also manifest itself when $D \ll I_0 \ll J_0$, i.e. even at weak anisotropy. This follows from Eq. (14). It can be seen that for $I_0 \ll J_0$, the value of D_c can be significantly less than I_0. This circumstance distinguishes SU3-F into a special class of quantum magnets in which quantum effects can show themselves not only at strong SIA.

5. Linearized Holstein–Primakoff transformation for F- and G-sublattices

The next step towards calculation of the energy spectrum in the SU3-F in the spin-wave approximation is to express the spin operators from F- and G-sublattices in terms of Bose operators. Since the spin dynamics in F- and G-subsystems involves only dipole degrees of freedom, the Holstein-Primakoff representation can be used for the operators S_f^α and S_g^α ($\alpha = \pm, z$):

$$\begin{aligned} &S_f^+ = \sqrt{2S - a_f^+ a_f}\ \ a_f, \quad S_f^z = S - a_f^+ a_f, \\ &S_g^+ = \sqrt{2S - b_g^+ b_g}\ \ b_g, \ S_g^z = S - b_f^+ b_g. \end{aligned} \tag{17}$$

Here Bose-operators $a_f(a_f^+)$ and $b_g(b_g^+)$ describe transitions between the states $|\uparrow'\rangle \leftrightarrow |\downarrow'\rangle$ and $|\uparrow''\rangle \leftrightarrow |\downarrow''\rangle$ with definite spin projections along the new quantization axes Oz' and Oz'' respectively (see Fig. 4a,b).

In terms of new variables, the operator $H(\theta)$ with quadratic accuracy in operators a_f and b_g has the form:

$$\begin{aligned} H(\theta) = &\sum_l H_0(l) \\ &+ I\sum_{\{fl\}}\left\{\cos\theta\left(\sqrt{\frac{S}{2}}(a_f + a_f^+)S_l^x - a_f^+ a_f S_l^z\right)\right. \\ &+ \sin\theta\left(\sqrt{\frac{S}{2}}(a_f + a_f^+)S_l^z + a_f^+ a_f S_l^x\right) \\ &\left.+ \frac{1}{i}\sqrt{\frac{S}{2}}(a_f - a_f^+)S_l^y\right\} \\ &+ I\sum_{\{gl\}}\left\{\cos\theta\left(\sqrt{\frac{S}{2}}(b_g + b_g^+)S_l^x - b_g^+ b_g S_l^z\right)\right. \\ &- \sin\theta\left(\sqrt{\frac{S}{2}}(b_g + b_g^+)S_l^z + b_g^+ b_g S_l^x\right) \\ &\left.+ \frac{1}{i}\sqrt{\frac{S}{2}}(b_g - b_g^+)S_l^y\right\} \\ &+ J\sum_{\{fg\}}\left\{\cos 2\theta\left(S^2 - Sa_f^+ a_f - Sb_g^+ b_g\right.\right. \\ &+ \frac{S}{2}(a_f + a_f^+)(b_g + b_g^+)\Big) \\ &- \frac{S}{2}(a_f - a_f^+)(b_g - b_g^+) \\ &\left.+ S\sqrt{\frac{S}{2}}\sin 2\theta\left(a_f + a_f^+ - b_g - b_g^+\right)\right\}, \end{aligned} \tag{18}$$

where the single-site operator

$$H_0(l) = D\left(S_l^y\right)^2 + \bar{H}\, S_l^z \tag{19}$$

from L-sublattice determines the non-equidistant energy levels of l-ions. Effective field

$$\bar{H} = 2I_0 S\cos\theta, \tag{20}$$

as noted above, may turn out to be small as compared to the anisotropy energy and then the non-diagonality of $H_0(l)$ becomes a significant factor. To take this circumstance into account, we take advantage of the Hubbard operators representation for spin operators S_l^α ($\alpha = \pm, z$)

$$\begin{aligned} &S_l^+ = \sqrt{2}\left(X_l^{1,0} + X_l^{0,-1}\right), \ S_l^- = \left(S_l^+\right)^+, \\ &S_l^z = X_l^{1,1} - X_l^{-1,-1}, \end{aligned} \tag{21}$$

where $X_l^{n,m} = |n,l\rangle\langle m,l|$, and the ket vectors are the eigenvectors of the operator S_l^z: $S_l^z|n,l\rangle = n|n,l\rangle$ ($n = -1, 0, +1$).

In the Hubbard operators representation, we get

$$\begin{aligned} H_0(l) = &\left(\frac{D}{2} - \bar{H}\right)X_l^{-1,-1} + DX_l^{00} \\ &+ \left(\frac{D}{2} + \bar{H}\right)X_l^{1,1} - \frac{D}{2}\left(X_l^{1,-1} + X_l^{-1,1}\right). \end{aligned} \tag{22}$$

The last term in Eq. (22) involves quadrupole degrees of freedom into dynamics.

6. $SU(3)$ transformation of the Hamiltonian

To diagonalize the operator $H_0(l)$ we use the approach developed in [45]. The idea of this approach is to employ the unitary operator

$$U_{1,-1}(\alpha, l) = \exp\left\{\alpha\, \Gamma_{1,-1}(l)\right\}, \tag{23}$$

with generator $\Gamma_{1,-1}(l) = X_l^{1,-1} - X_l^{-1,1}$ and a real variational parameter α, to express the Hubbard operators X_l^{nm} ($n, m = -1, 0, +1$) through the new ones as (see Appendix B):

$$X_l^{nm} = U_{\tilde{1},-\tilde{1}}(\alpha, l) X_l^{\tilde{n}\tilde{m}} U_{\tilde{1},-\tilde{1}}^+(\alpha, l). \tag{24}$$

When writing this expression the equality $U_{\tilde{1},-\tilde{1}}(\alpha, l) = U_{1,-1}(\alpha, l)$ was taken into account. The new Hubbard operators $X_l^{\tilde{n}\tilde{m}}$ are defined in terms of new states: $X_l^{\tilde{n}\tilde{m}} = |\tilde{n}, l\rangle\langle\tilde{m}, l|$, where the new states, according to Eq. (B.2), are expressed via the initial ones as follows

$$|\tilde{n}, l\rangle = U_{1,-1}(-\alpha, l)|n, l\rangle. \tag{25}$$

Taking into account Eq. (B.1) we get

$$|+\tilde{1}\rangle = \cos\alpha\,|+1\rangle + \sin\alpha\,|-1\rangle,$$

$$|\tilde{0}\rangle = |0\rangle,$$
$$|-\tilde{1}\rangle = \cos\alpha\,|-1\rangle - \sin\alpha\,|+1\rangle. \tag{26}$$

It is seen that the state $|+\tilde{1}\rangle$ is nothing but the state $|\psi\rangle$ in En. (8) that was guessed in Ref. [8].

With regard to the Hamiltonian (18), the substitution of Eq. (24) for Hubbard operators can be represented formally as $SU(3)$-transformation (see Ref. [45]):

$$H(\theta) \to H(\theta,\alpha) = U_3(\alpha)\,H(\theta)\,U_3^{\dagger}(\alpha), \tag{27}$$

with the unitary operator:

$$U_3(\alpha) = \prod_{l\in L} U_{1,-1}(\alpha, l). \tag{28}$$

Eqs. (24) with right hand side evaluated explicitly for different indices n and m are summarized in Eq. (B.6). Substituting these expressions into Eq. (22) and requiring the coefficients for non-diagonal new Hubbard operators to vanish, we obtain the following diagonal form for the transformed single-site Hamiltonian:

$$H_0(l,\alpha) = \varepsilon_{-1}X_l^{-\tilde{1},-\tilde{1}} + \varepsilon_0 X_l^{\tilde{0}\tilde{0}} + \varepsilon_1 X_l^{\tilde{1}\tilde{1}}, \tag{29}$$

where

$$\begin{aligned}\varepsilon_{-1} &= \frac{D}{2}(1+\sin 2\alpha) + |\bar{H}|\cos 2\alpha,\\ \varepsilon_0 &= D,\\ \varepsilon_1 &= \frac{D}{2}(1-\sin 2\alpha) - |\bar{H}|\cos 2\alpha.\end{aligned} \tag{30}$$

The equation for determining angle α turns out to be trivial: $D\cos 2\alpha = -2\bar{H}\sin 2\alpha$, and expressions for trigonometric functions of interest are as follows

$$\begin{aligned}\sin\alpha &= \sqrt{\frac{1}{2} - \frac{|\bar{H}|}{\nu}}, \quad \sin 2\alpha = \frac{D}{\nu},\\ \cos\alpha &= \sqrt{\frac{1}{2} + \frac{|\bar{H}|}{\nu}}, \quad \cos 2\alpha = \frac{2|\bar{H}|}{\nu},\\ \nu &= \sqrt{D^2 + 4\bar{H}^2}.\end{aligned} \tag{31}$$

Given these expressions, the eigenvalues (30) of the single-site Hamiltonian $H_0(l,\alpha)$ can be rewritten as:

$$\varepsilon_{-1} = \frac{D+\nu}{2}, \quad \varepsilon_0 = D, \quad \varepsilon_1 = \frac{D-\nu}{2}. \tag{32}$$

When $\bar{H} = 0$ the energy $\varepsilon_1 = 0$ and $\varepsilon_{-1} = \varepsilon_0 = D$.

The expression for transformed total Hamiltonian (27), obtained as a result of substituting Eqs. (24) (or rather Eqs. (B.6)) into the operator $H(\theta)$ as it was done above for $H_0(l)$, is not shown here due to its bulkiness, but in the next Section we write it out after introducing the Bose operators acting in the Hilbert subspace of L-sublattice.

7. Bosonization of the L subsystem

The single-site Hamiltonian (29) describes a three-level system in terms of the new Hubbard operators (Fig. 4c). At low temperatures it is more convenient to take advantage of Bose operators description of the Hamiltonian instead of Hubbard ones due to rather complicated commutation relations of the latter. To this end, following the Refs. [7, 11,46] we introduce two new kinds of bosons (c and d). Creation of a boson at the site l, by means of the Bose operators c_l^+ or d_l^+, imply transition of the three-level system from the ground state $|+\tilde{1}\rangle$ to the excited state $|\tilde{0}\rangle = c_l^+|+\tilde{1}\rangle$ or $|-\tilde{1}\rangle = d_l^+|+\tilde{1}\rangle$, respectively. The states with a larger number of bosons are cut off as non-physical by the metric operator.

The new Hubbard operators $X^{\bar{p}\bar{q}}$ $(p,q = 1,0,-1)$, according to Refs. [7,46], are expressed in terms of boson operators as follows:

$$\begin{aligned}X^{\tilde{0},\tilde{1}} &= c^+, \qquad X^{\tilde{1},\tilde{0}} = (1 - c^+c - d^+d)\,c,\\ X^{-\tilde{1},\tilde{1}} &= d^+, \qquad X^{\tilde{1},-\tilde{1}} = (1 - c^+c - d^+d)\,d,\end{aligned}$$

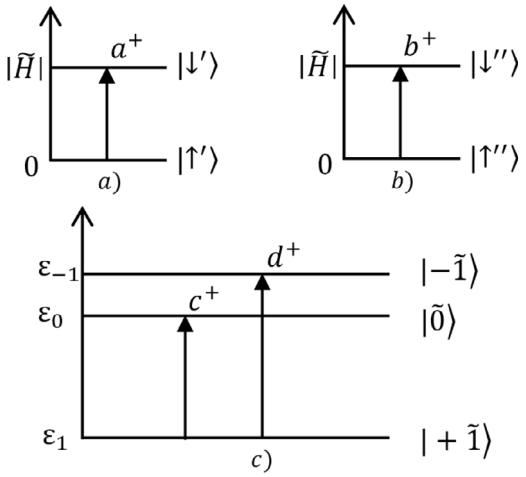

Fig. 4. Energy diagrams describing the action of Bose-operators: (a) operator a_f^+ in F-sublattice; (b) operator b_f^+ in G-sublattice; (c) operators c_f^+ and d_f^+ in the three-level system of L-sublattice described by the Hamiltonian $H_0(l,\alpha)$. Definitions of all the states and energies used are given after Eq. (17) and in Eqs. (26), (32), (35).

$$\begin{aligned}X^{\tilde{1},\tilde{1}} &= (1 - c^+c - d^+d), \qquad X^{\tilde{0},\tilde{0}} = c^+c,\\ X^{-\tilde{1},-\tilde{1}} &= d^+d, \quad X^{\tilde{0},-\tilde{1}} = c^+d, \quad X^{-\tilde{1},\tilde{0}} = d^+c.\end{aligned} \tag{33}$$

Using these expressions together with Eqs. (B.7), relating the spin and Hubbard operators, the transformed Hamiltonian (27) can be represented in the form:

$$\begin{aligned}H &= E_G + E_c\sum_l c_l^+c_l + E_d\sum_l d_l^+d_l\\ &\quad - \tilde{H}\sum_f a_f^+a_f - \tilde{H}\sum_g b_g^+b_g\\ &\quad + \frac{JS}{2}\sum_{\{fg\}}\Big(\cos 2\theta\,(a_f + a_f^+)(b_g + b_g^+)\\ &\quad - (a_f - a_f^+)(b_g - b_g^+)\Big)\\ &\quad + I\sqrt{\frac{S}{2}}\sum_{\{fl\}}\Big(\phi_+\cos\theta\,(a_f + a_f^+)(c_l + c_l^+)\\ &\quad - \phi_-(a_f - a_f^+)(c_l - c_l^+)\\ &\quad - \sin\theta\sin 2\alpha\,(a_f + a_f^+)(d_l + d_l^+)\Big)\\ &\quad + I\sqrt{\frac{S}{2}}\sum_{\{gl\}}\Big(\phi_+\cos\theta\,(b_g + b_g^+)(c_l + c_l^+)\\ &\quad - \phi_-(b_g - b_g^+)(c_l - c_l^+)\\ &\quad + \sin\theta\sin 2\alpha\,(b_g + b_g^+)(d_l + d_l^+)\Big),\end{aligned} \tag{34}$$

where

$$\begin{aligned}&E_c = \varepsilon_0 - \varepsilon_1 = \frac{D+\nu}{2}, \quad E_d = \varepsilon_{-1} - \varepsilon_1 = \nu,\\ &\tilde{H} = J_0S\cos 2\theta + I_0\cos\theta\cos 2\alpha,\\ &\phi_\pm = (\cos\alpha \pm \sin\alpha)/\sqrt{2},\\ &E_G = N(\varepsilon_1 + J_0S^2\cos 2\theta),\end{aligned} \tag{35}$$

and N is a number of sites in sublattice.

When writing the expression (34), only terms not higher than the second degree in Bose operators were left. Besides, the coefficients before the terms of the first degree were set to zero. This gives the equation for determining the angle θ:

$$\cos\theta = -I_0\cos 2\alpha/2J_0S, \tag{36}$$

which is consistent with the previously given expressions (10) and (15). The Eq. (36) together with the Eqs. (31) for $\cos 2\alpha$ and (20) for $\bar{H}$ form

a system with solutions

$$\cos 2\alpha = \sqrt{1-\left(\frac{D}{D_c}\right)^2}, \tag{37}$$

$$\cos\theta = -\frac{I_0}{2J_0 S}\sqrt{1-\left(\frac{D}{D_c}\right)^2}, \tag{38}$$

coinciding with that of (15) obtained earlier in the mean field approximation. The value of D_c (see Eq. (14)) defines the upper bound for parameter D for which there are nontrivial solutions for the angles α and θ corresponding to the canted ferrimagnetic phase. At $D > D_c$, the system enters a quadrupole antiferromagnetic phase (see below) in which angles stay constant and equal: $\alpha = \pi/4$, $\theta = \pi/2$.

8. The dispersion equation

In the quasi-momentum representation, the Hamiltonian (34) takes the compact form:

$$\begin{aligned}
H = \sum_k \{ & E_c\, c_k^+ c_k + E_d\, d_k^+ d_k - \tilde{H} a_k^+ a_k - \tilde{H} b_k^+ b_k \\
& + I_- \left[\gamma_k a_k c_{-k} + \gamma_k^* a_k^+ c_{-k}^+ + \gamma_k^* b_k c_{-k} + \gamma_k b_k^+ c_{-k}^+\right] \\
& + I_+ \left[\gamma_k^* a_k^+ c_k + \gamma_k c_k^+ a_k + \gamma_k b_k^+ c_k + \gamma_k^* c_k^+ b_k\right] \\
& + I_d \left[\gamma_k^* b_k d_{-k} + \gamma_k b_k^+ d_{-k}^+ - \gamma_k a_k d_{-k} - \gamma_k^* a_k^+ d_{-k}^+\right. \\
& + \left.\gamma_k b_k^+ d_k + \gamma_k^* d_k^+ b_k - \gamma_k^* a_k^+ d_k - \gamma_k d_k^+ a_k\right] \\
& + J_- \left[\gamma_k^* a_k b_{-k} + \gamma_k a_k^+ b_{-k}^+\right] \\
& + J_+ \left[\gamma_k a_k^+ b_k + \gamma_k^* b_k^+ a_k\right]\} + E_G,
\end{aligned} \tag{39}$$

where

$$\begin{aligned}
I_\pm &= I_0\sqrt{\frac{S}{2}}\,(\phi_+ \cos\theta \pm \phi_-), \\
I_d &= I_0\sqrt{\frac{S}{2}}\,\sin\theta\,\sin 2\alpha, \\
J_\pm &= J_0\,\frac{S}{2}\,(\cos 2\theta \pm 1), \\
\gamma_k &= \frac{1}{3}\sum_\delta e^{ik\delta} = \frac{1}{3}\left(2\cos\frac{k_z}{2}\, e^{\,i\frac{k_x}{2\sqrt{3}}} + e^{-i\frac{k_x}{\sqrt{3}}}\right).
\end{aligned} \tag{40}$$

In the last expression, the vector δ runs over three values $\{\xi,\ -\zeta,\ \zeta-\xi\}$ (Fig. 1). These three vectors connect each site of $L(F(G))$-sublattice with three nearest sites from $F(G(L))$-sublattice. Similarly, three vectors $-\delta$ connect each site of $L(F(G))$-sublattice with three nearest sites from $G(L(F))$-sublattice.

To calculate the spectrum of collective spin excitations, we introduce the matrix retarded Green's function $\langle\langle \mathbf{X}_k^\dagger | \mathbf{X}_k \rangle\rangle_\omega$, where

$$\mathbf{X}_k = (a_k^+, b_k^+, c_k^+, d_k^+, a_{-k}, b_{-k}, c_{-k}, d_{-k}).$$

By writing out the equations of motion for this function and requiring the existence of nontrivial solutions, we obtain the dispersion equation:

$$\begin{vmatrix} \omega - \mathbf{A}_k & -\mathbf{B}_k \\ \mathbf{B}_k & \omega + \mathbf{A}_k \end{vmatrix} = 0, \tag{41}$$

where

$$\mathbf{A}_k = \begin{pmatrix} -\tilde{H} & J_+\gamma_k & I_+\gamma_k^* & -I_d\gamma_k^* \\ J_+\gamma_k^* & -\tilde{H} & I_+\gamma_k & I_d\gamma_k \\ I_+\gamma_k & I_+\gamma_k^* & E_c & 0 \\ -I_d\gamma_k & I_d\gamma_k^* & 0 & E_d \end{pmatrix}, \tag{42}$$

and

$$\mathbf{B}_k = \begin{pmatrix} 0 & J_-\gamma_k & I_-\gamma_k^* & -I_d\gamma_k^* \\ J_-\gamma_k^* & 0 & I_-\gamma_k & I_d\gamma_k \\ I_-\gamma_k & I_-\gamma_k^* & 0 & 0 \\ -I_d\gamma_k & I_d\gamma_k^* & 0 & 0 \end{pmatrix}. \tag{43}$$

The dispersion equation (41) is an equation of the fourth degree with respect to ω^2, and its solutions represent four branches of the spectrum of collective spin excitations of the three-lattice SU3-F.

When the value of the SIA-parameter D exceeds the critical value D_c, the SU3-F turns out to be in the QAFM phase, and Eq. (41) is significantly simplified. In this case, for the four branches of spin-wave excitations the following analytical expressions can be obtained:

$$\begin{aligned}
\epsilon_1(k) &= J_0 S\sqrt{1-|\gamma_k|^2}, \\
\epsilon_2(k) &= \sqrt{\left(\epsilon_1(k)^2 + D^2 - \Lambda_k^2\right)/2}, \\
\epsilon_3(k) &= D, \\
\epsilon_4(k) &= \sqrt{\left(\epsilon_1(k)^2 + D^2 + \Lambda_k^2\right)/2},
\end{aligned} \tag{44}$$

where

$$\begin{aligned}
\Lambda_k^2 &= \sqrt{(\epsilon_1(k)^2 - D^2)^2 + 8S^2 I_0^2 J_0 D\Gamma_k}, \\
\Gamma_k &= 2|\gamma_k|^2 - 2\,\mathrm{Re}\{{\gamma_k}^3\}.
\end{aligned} \tag{45}$$

Note that in Eqs. (44) the third non-dispersive branch $\epsilon_3(k)$ describes the energy of localized d-boson excitations at $D > D_c$.

In the following Sections, the obtained expressions are used to determine the ground state magnetic structure and spectral characteristics of the SU3-F.

9. Ground state magnetic structure. Dipole and quadrupole order parameters

As it was noted, at large values of SIA, as an order parameter in quantum magnets should be considered not only the dipole moment (i.e., the magnetic moment of one ion in a separate sublattice), but also a quadrupole moment (11).

The average value of the magnetic moment R for F- and G-sublattices in the spin-wave approximation can be calculated using the formula:

$$R = \langle S_f^z \rangle = \langle S_g^z \rangle = S - n_a, \tag{46}$$

following from the definitions (17). In the case of L sublattice, the expression for $R_L = \langle S_l^z \rangle$ is obtained from Eq. (B.7) after replacing in it the Hubbard operators with Bose operators according to (33):

$$R_L = \cos 2\alpha \cdot (1 - n_c - 2\,n_d). \tag{47}$$

The average number of bosons n_ρ of type $\rho = a, b, c, d$ in Eqs. (46) and (47) is determined by the expression:

$$n_\rho = \frac{1}{N}\sum_k \langle \rho_k^+ \rho_k \rangle, \tag{48}$$

and is calculated by means of spectral theorem applied to the corresponding component of the matrix Green's function $\langle\langle \mathbf{X}_k^\dagger | \mathbf{X}_k \rangle\rangle_\omega$.

It can be seen that the expression (47) for the order parameter R_L differs from the expression (10) for R_L^{MF} in the mean field approximation by additional fluctuation terms affecting the magnitude of the quantum spin reduction in the L-sublattice.

The expression for the average value of the quadrupole moment (11) is obtained similarly to formula (47). Sequentially using the representations (B.7) and (33) to derive the square of the operator S_l^y, we find:

$$Q_2^0 = \frac{3}{2}(1 + n_c) - \frac{3}{2}\sin 2\alpha(1 - n_c - 2n_d) - 2. \tag{49}$$

This expression also differs from the formula (12) for Q^{MF}, obtained in the mean field approximation, by the quantum fluctuation corrections.

Another quantity that bears important information is the total magnetic moment M. It is natural to define it as the projection of the vector sum $\mathbf{R}_F + \mathbf{R}_G + \mathbf{R}_L$ onto the axis Oz:

$$M = R_L + 2R\cos\theta. \tag{50}$$

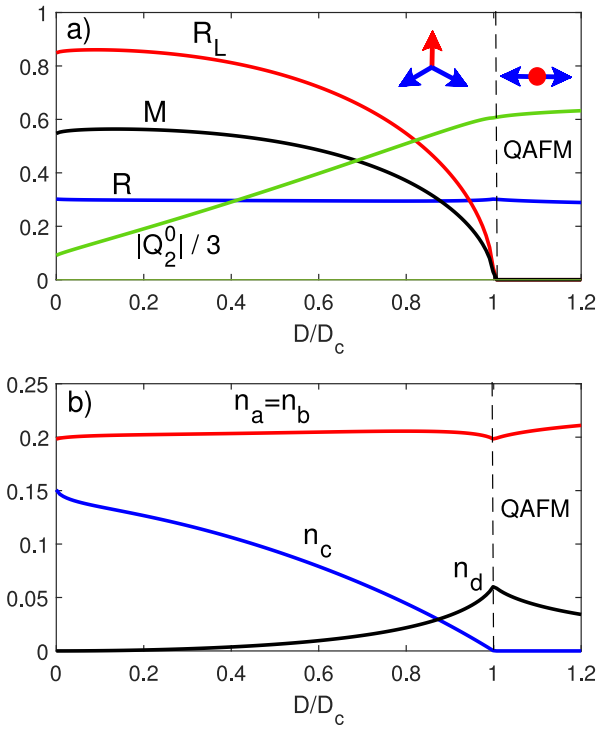

Fig. 5. (a) Dependencies of the quantities R_L (red curve), R (blue curve), M (black curve) and $|Q_2^0|$ (green curve) on the parameter D. For convenience, the value of $|Q_2^0|$ has been reduced three times. (b) Dependencies of the boson numbers n_ρ ($\rho = a, b, c, d$) on the SIA-parameter D. The exchange integrals ratio is $I/J = 0.5$. At the same time, $D_c/J = 1.5$.

The vector **M** in the chosen coordinate system is always directed along the z-axis (Fig. 1).

Calculation of four quantities R, R_L, Q_2^0 and M was carried out at zero temperature. The results of numerical calculations depend significantly on the ratio of the exchange integrals I and J.

We start with the case of weak exchange coupling I. Let us take $I/J = 1/2$. With this chosen ratio of I/J and with $D = 0$, the equilibrium angle θ turns out to be 120^0. Thus, all three angles between three equilibrium coplanar sublattice magnetizations are equal. This is because the exchange integral I, being twice as small as J, describes the interaction between sublattices in one of which the spin is twice as large as in another. As a result, the energy of the exchange interactions between all three pairs of the three sublattices turns out to be the same.

The dependencies of the total magnetic moment M, the quadrupole moment Q_2^0, as well as the moments of the sublattices R_L and R on the anisotropy parameter D at the ratio $I/J = 0.5$ are shown in Fig. 5a. It can be seen that spins in all three sublattices reveal significant reduction due to quantum fluctuations. However, while the value of R does not change significantly with an increase in D, the values of R_L and M turn to zero at $D = D_c$ according to the square root law. At the same time, the angle of θ decreases from 120^0 to 90^0. In its turn, the quadrupole moment of the L-sublattice Q_2^0, with increase in the SIA-parameter, demonstrates monotonic increase (in absolute value, since $Q_2^0 < 0$) with saturation at the point $D = D_c$. Zeroing out of the parameters R_L and M, as well as saturation of the value Q_2^0, means that at the point $D = D_c$ the system enters the QAFM phase. In this case, the spins of the L-sublattices are characterized by a quadrupole ordering and the magnetic moments of the other two sublattices are equal in modulus and antiparallel.

The described behavior is illustrated in Fig. 5a by two pictograms which show the magnetic structure of SU3-F to the left and right of the critical point $D = D_c$. Position of this point is indicated by a vertical dashed line. Using a red circle instead of an arrow symbolizes turning R_L to zero.

Fig. 5b shows the dependence of the boson numbers of each type on the magnitude of anisotropy parameter D. The character of these dependencies significantly affects the shape of the curves in Fig. 5a. It can be seen that for $D = 0$ the value of n_c is finite and $n_d = 0$. This means that due to exchange interactions only the state $|\tilde{0}\rangle$ is mixed to the ground single-ion state $|+\tilde{1}\rangle$ (Fig. 4c). On the contrary, for $D = D_c$ the value of n_d is finite and $n_c = 0$. In this case, only the state $|-\tilde{1}\rangle$ is mixed to the ground state $|+\tilde{1}\rangle$. It is precisely the sharp decrease in the number of n_c in the vicinity of small values of D that explains the slight increase in the parameter R_L at the origin (the red curve in Fig. 5a). The numbers of a and b bosons that determine the spin quantum reduction in F and G sublattices depend weakly on the anisotropy parameter D.

At $D = 0$, an increase in the exchange integral I makes the equilibrium angle θ to increase so that at $I = J$ the angle turns out to be equal to 180^0: the magnetic moments of both F- and G-sublattices in this case are directed against the Oz axis and together compensate completely the magnetic moment of the L-sublattice (leading to $M = 0$). Note that this compensation point appears despite the fact that the spins of all three sublattices undergo quantum reduction. This can be seen from Fig. 6a, which shows the dependence of the magnetic moments R_L, R and M on the value of SIA. Comparison of these dependencies with the similar curves in Fig. 5a shows that increase in I leads to: (1) decrease in the spin quantum reduction in the F- and G-sublattices (blue line); (2) more pronounced increase in R_L in the vicinity of the origin (red line); (3) the most important, the total magnetic moment M now turns to zero at two values of the SIA-parameter: $D = 0$ and $D = D_c$ (black line in Fig. 6a). In the first case ($D = 0$), as was already said, the magnetic moments of all three sublattices are nonzero. However, while the moment in the L-sublattice is oriented along Oz axis, in the F- and G-sublattices it is oriented against Oz. In this phase, the moments of the three sublattices completely compensate each other. In the second case ($D = D_c$), we have $R_L = 0$ but magnetic moments in F- and G-sublattices are directed opposite to each other and parallel to the Ox axis, and also add up to $M = 0$. For all intermediate values of the SIA-parameter, the system is in canted ferrimagnetic phase (see the pictogram in Fig. 6a), and the total magnetic moment is nonzero and points along the positive direction of Oz axis. The quadrupole order parameter Q_2^0, as in the case of $I < J$, increases monotonously in absolute value and at $D \geqslant D_c$, in the domain corresponding to the QAFM phase, saturates up to maximum values. A minor difference from the previous case, shown in Fig. 5a, is due to the fact that now, the green curve, describing the dependence of Q_2^0 on D, starts at the origin, so that at $D = 0$ the quadrupole order parameter Q_2^0 is zero.

The dependencies of the boson numbers on the anisotropy parameter D at $I/J = 1$ are shown in Fig. 6b. It can be seen that an increase in the exchange integral I leads to a decrease in the boson numbers n_a and n_b, which, in turn, causes a decrease in the quantum spin reduction in the F- and G-sublattices. Otherwise, the dependencies of n_ρ ($\rho = a, b, c, d$) on the SIA-parameter qualitatively repeat similar curves in Fig. 5b.

The most interesting situation arises when the values of the exchange integral I are greater than that of J. The results of calculations for $I/J = 1.2$ are shown in Fig. 7. It can be seen from Fig. 7a that, unlike the previously considered relations between I and J, now the projection M of the total moment on the Oz-axis turns out to be negative when the ratio D/D_c ranges from 0.1 to 0.762 (the red dots on the black curve) and positive (or zero) for D/D_c outside of this interval. This behavior is explained by the reversal of the magnetic moments in F- and G-sublattices and the specific D dependence of the boson numbers n_ρ ($\rho = a, b, c, d$), which determine the R and R_L values. Inflection of the curves describing the corresponding dependencies in Figs. 7a and 7b at the point $D_* \cong 0.54\, D_c$ (blue dots on the abscissa axes) is due to the sudden decrease in the equilibrium angle θ. This angle on the entire interval to the left of the point D_* is constant and

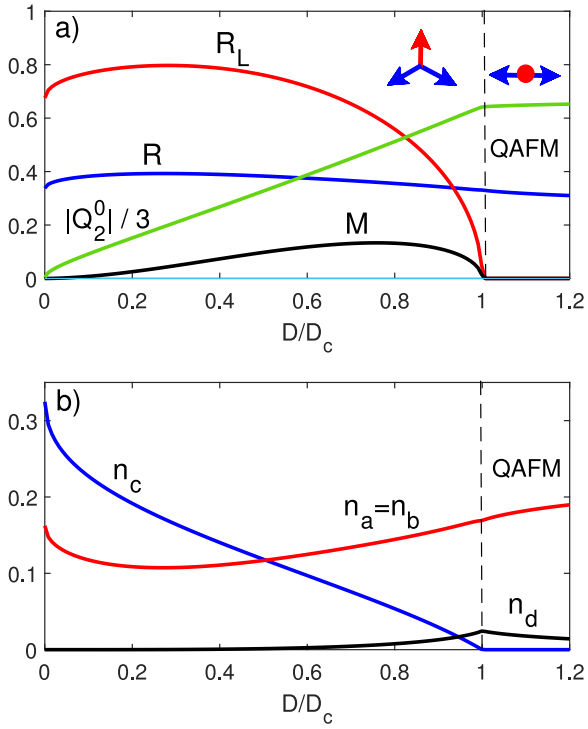

Fig. 6. (a) The dependence of quantities R_L (red curve), R (blue curve), M (black curve) and $|Q_2^0|$ (green curve) on the parameter D. (b) The dependence of boson numbers n_ρ ($\rho = a, b, c, d$) on the parameter of SIA. The ratio of exchange integrals is $I/J = 1$. The critical value of SIA: $D_c = 6J$.

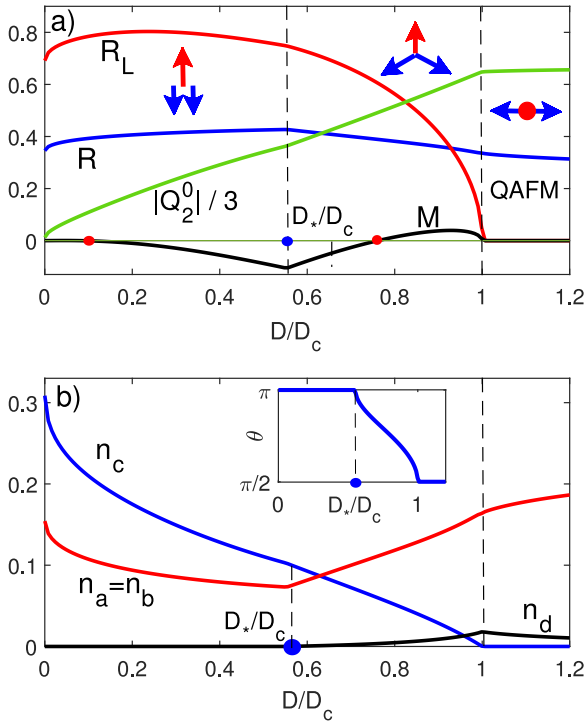

Fig. 7. (a) The dependence of quantities R_L (red curve), R (blue curve), M (black curve) and $|Q_2^0|$ (green curve) on the parameter D. (b) The dependence of boson numbers n_ρ ($\rho = a, b, c, d$) on the SIA-parameter. The ratio of exchange integrals is $I/J = 1.2$. In this case, $D_c/J = 8.64$. The inset in the lower plot demonstrates dependence of the angle θ on the SIA-parameter. The magnitude of the anisotropy parameter D_*, corresponding to the beginning of canting of the magnetic moments in F- and G-sublattices, is indicated by blue dots on the abscissa axes.

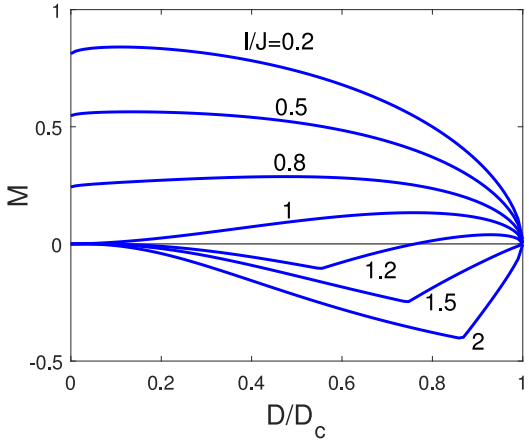

Fig. 8. Dependencies of the total magnetic moment M on the SIA-parameter D at different ratios between the exchange integrals I and J. The values of I/J are indicated nearby the corresponding curves.

is equal to 180^0, but on the right side of D_* — decreases monotonously and at $D = D_c$ takes the value 90^0 (see insert on Fig. 7b).

Thus, if for $I = J$ the collinear spin configuration (when $\mathbf{R}_L$ is directed along the Oz axis, and $\mathbf{R}_F$ and $\mathbf{R}_G$ are directed oppositely) occurred only at one value of D equal to zero (see discussion of Fig. 6a), now, for $I > J$, this collinear configuration persists in the whole range of D values from zero to D_*. The domains corresponding to the three specified magnetic configurations: collinear ferrimagnetic, canted ferrimagnetic, and quadrupole antiferromagnetic, are indicated in Fig. 7a by corresponding pictograms.

The dependence of the quadrupole order parameter Q_2^0 on the SIA-parameter D (the green line in Fig. 7a) repeats a similar dependence at $I = J$ in Fig. 6a.

Fig. 8 demonstrates the projection M of the total magnetization on the Oz-axis as a function of the anisotropy parameter D for several values of I/J.

To the right of D_c, the SU3-F is in the QAFM phase at all the ratios I/J. Therefore, for $D \geqslant D_c$, the projection of M is identically zero. For $I < J$, at any value of the parameter D from the range $[0, D_c)$ only the canted ferrimagnetic state is implemented ($\theta < \pi$). In this case, for all values of $D < D_c$, the projection of M is nonzero and positive. The minimum value of the exchange integral I at which a collinear ($\theta = 0$) ferrimagnetic phase occurs is J. Moreover, at $I = J$, this phase occurs only at one point $D = 0$, and it is at this point (from the entire interval $[0, D_c)$) the value of M turns out to be zero for the first time. With a further increase in the exchange integral I, the range of collinear ferrimagnetic phase increases and is characterized by the interval $[0, D_*)$, where the value of D_*, separating the collinear and canted phases, can be visually identified as the inflection point on the dependencies $M(D)$ (see the three lower curves in Fig. 8, calculated for $I/J = 1.2$, 1.5 and 2). It can also be seen from the figure that at the point $D = 0$ the projection M of the total magnetization remains equal to zero for all $I > J$.

An important fact following from the analysis of the curves in Fig. 8 consists in changing the sign of the projection of the total magnetic moment M as soon as the ratio I/J becomes greater than one. The direction of the moment $\mathbf{M}$ is reversed not by rotating the vector $\mathbf{M}$, but by reducing its length to zero and then increasing in the opposite direction. The sign change of M may occur at any value of D from $(0, D_c)$, but not necessarily for the same value of the ratio I/J. As a result, the situation discussed above in Fig. 7a for $I/J = 1.2$ may arise, in which the sign of M changes twice as D increases leading in this way to two compensation points.

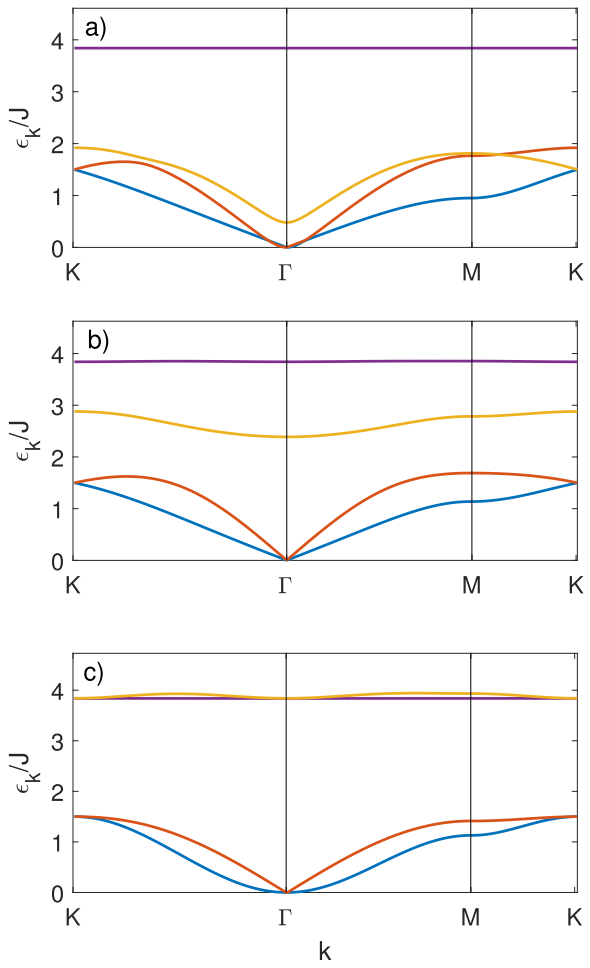

Fig. 9. Spin-wave excitation spectrum at $I/J = 0.8$ and three anisotropy parameter values: (a) $D = 0$; (b) $D = 0.5D_c$ and (c) $D = D_c$. In this case $D_c/J = 3.84$. The position of the points Γ, K and M is indicated in Fig. 10.

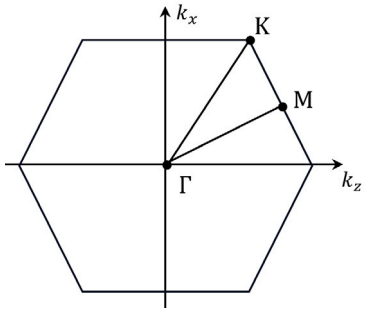

Fig. 10. Brillouin zone of triangular lattice and high-symmetry points.

10. Spin-wave excitation spectrum in SU3-F

Fig. 9 demonstrates the spin-wave spectrum at $I/J = 0.8$ for three values of the SIA-parameter: $D/D_c = 0$, 0.5 and 1. The wave vector k runs through a triangle formed by the points Γ, K and M in the Brillouin zone. The position of these points is shown in Fig. 10.

It can be seen that at $D = 0$ (Fig. 9a) there are two gapless branches (blue and red) that turn to zero at $k = 0$. The other two branches (yellow and purple) describe excitations with finite energy for all wave vectors k. At the same time, the highest-energy and almost non-dispersed violet branch corresponds to d boson excitations with energy E_d(35).

As the anisotropy parameter increases, the yellow (gaped) branch moves upward (Fig. 9b) and at $D = D_c$ almost merges with the high-energy purple one (Fig. 9c).

The described behavior of the yellow dispersion curve in Fig. 9 correlates with the change in the angle θ. As was noted in the previous Section (see also expression (38)) for $I/J < 1$, the angle θ is less than π for any value of D. In this case, the excitation spectrum showed by the yellow curve is gaped for all the values of D. At $D = 0$, the angle θ acquires maximal value and the gap is minimal (Fig. 9a). As the SIA-parameter increases, the angle θ, in accordance with discussion in the previous Section, decreases, reaching the minimum value $\pi/2$ at $D = D_c$, and the gap, on the contrary, increases and turns out to be maximal at $D = D_c$ (Fig. 9c).

Given the described correlation between the angle θ and the gap width for yellow dispersion curve, we can expect the gap to turn to zero at $\theta = \pi$. This is possible for $I \geqslant J$.

Fig. 11 shows the results of calculations of the spin-wave excitation spectrum at equal exchange integrals ($I = J$) for three values of the anisotropy parameter D. As noted above, when the exchange parameters I and J are equal, the angle θ is equal to π at only one point: $D = 0$ (see the formula (38)). And it is at this point, as expected, the yellow dispersion curve turns out to be gapless (Fig. 11a). For any other values of D the gap is finite. The absence of a gap in the yellow dispersion curve in Fig. 11a is the main feature that distinguishes it from the similar curve in Fig. 9a. At other (non-zero) parameters of the SIA, the dispersion curves in Figs. 9 and 11, calculated respectively at $I/J = 0.8$ and $I/J = 1$ exhibit similar dynamics with an increase in D: two branches remain gapless and one (yellow) goes upward. At $D = D_c$, yellow curve merges with the dispersionless high-energy purple curve with energy E_d.

The latter fact means that the excitations described by the yellow and purple dispersion curves are of the same nature. Since, as noted above, the purple branch corresponds to the d-boson excitations, the yellow one should be associated with the c-boson excitations. Both of these boson types are due to excitations in the L-subsystem (with $S = 1$), which at $D = D_c$ enters the quadrupole phase with $R_L = 0$.

The most interesting modification of the dispersion curves with a change in the parameter D occurs at $I/J > 1$. Fig. 12 shows an example of such a modification at the ratio of exchange integrals $I/J = 1.2$. At zero value of the anisotropy parameter (Fig. 12a), only two of the four dispersion curves are gapless (there are three such curves in Fig. 11a). One of them, yellow, is associated with c-boson excitations, as before, with an increase in D becomes gaped, goes up and, eventually, merges with the purple disperseless branch describing d-boson excitations.

The second gapless branch (red in Fig. 12) changes insignificantly and remains gapless at all values of the SIA-parameter. This branch corresponds to the Goldstone mode associated with the violation of continuous symmetry with respect to rotation around the axis Oy normal to the plane of the triangular lattice under consideration (Fig. 3).

Peculiar behavior in Fig. 12 is demonstrated by the blue dispersion curve. At $D = 0$ (Fig. 12a), this curve describes spin-wave excitations with finite energy for all k. Let us denote by Δ_0 the minimum energy of these excitations at $k = 0$. When the parameter D is increased, the gap Δ_0 begins to decrease (see Figs. 12b, 12c) and at some value of $D = D_*$ turns to zero (Fig. 12d). With a further increase in D, the blue curve remains gapless for all D in the range from D_* to D_c (Figs. 12d, 12e, 12f). The described behavior of the gap Δ_0 as a function of the SIA-parameter is shown in Fig. 13.

Transformation of the blue dispersion curve shown in Fig. 12, and in particular the character of change of the gap width at $k = 0$ (Fig. 13), allow us to conclude that the excitations described by this curve are associated with the rotation of magnetic moments in F- and G-sublattices around the Oz axis parallel to the L-sublattice magnetic moment (Fig. 3). Indeed, for $D \in (D_*, D_c)$ the system is in canted ferrimagnetic phase (angle $\theta < \pi$). Since in the ground state under consideration, the magnetic moments of all spins from the L sublattice

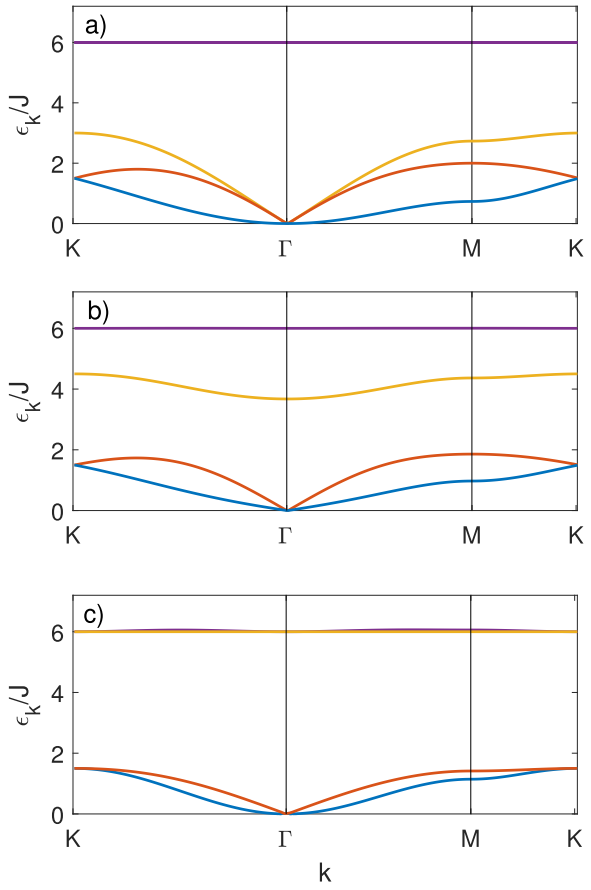

Fig. 11. Spin-wave excitation spectrum at $I = J$ and three values of the anisotropy parameter: (a) $D = 0$, (b) $D = D_c/2$, (c) $D = D_c$. In this case $D_c/J = 6$. The position of the points Γ, K and M is indicated in Fig. 10.

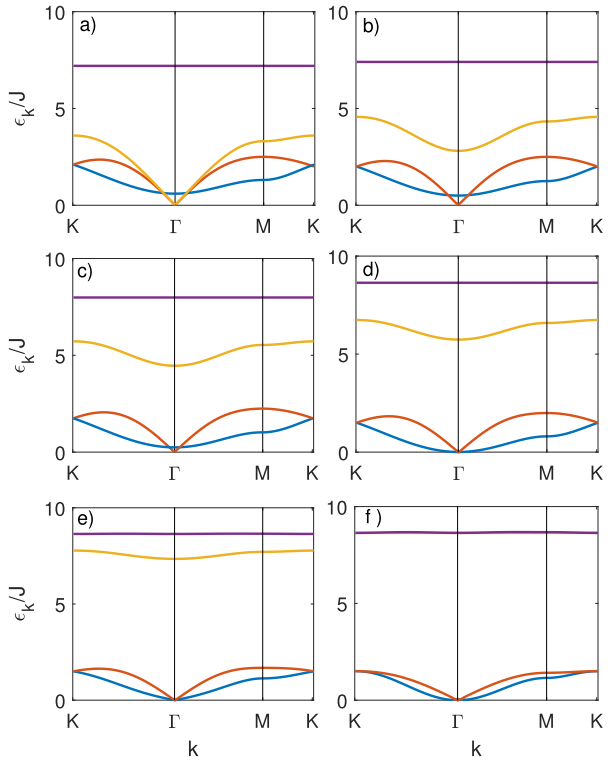

Fig. 12. Spin-wave excitation spectrum at $I/J = 1.2$. Anisotropy parameter: (a) $D = 0$; (b) $D = 0.2D_c$; (c) $D = 0.4D_c$; (d) $D = D_* = 0.56D_c$; (e) $D = 0.8D_c$; (f) $D/D_c = 1$. In this case $D_c/J = 8.64$. The position of the points Γ, K and M is indicated in Fig. 10.

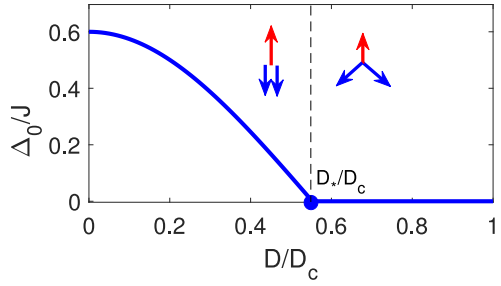

Fig. 13. The gap Δ_0 (see the text) as a function of SIA-parameter at $I/J = 1.2$.

are oriented parallel to each other and along the Oz axis, the energy of the system turns out to be invariant with respect to rotation around the Oz axis of two vectors $\mathbf{R}_F$ and $\mathbf{R}_G$ by arbitrary but identical angle. For Hamiltonian, such an invariance, according to the Goldstone theorem, would mean the existence of a gapless mode associated with violation of continuous symmetry with respect to rotation about the Oz axis of the plane formed by this axis and the vectors $\mathbf{R}_F$ and $\mathbf{R}_G$. Since in our case we can only talk about the invariance of the average energy (not the Hamilton operator) and, moreover, in a specific canted ferrimagnetic ground state, then the gapless blue dispersion curve in Fig. 12, at the specified range of D, is not a Goldstone mode in the strict sense. Nevertheless, the behavior of this curve obeys the conditions of the Goldstone theorem. In particular, at $D < D_*$, when the system is in ferrimagnetic collinear phase (the moments of all three sublattices are parallel to the Oz axis), the ground state does not violate the specified energy symmetry. Such a statement in respect to the Hamiltonian, according to the Goldstone theorem, would mean that there is no need for a corresponding gapless mode. As can be seen from Figs. 12 and 13, the behavior of the blue dispersion curve exactly satisfies these requirements.

An important question which cannot be answered unambiguously within only numerical calculations is the character of k-dependence of the blue dispersion curve in the vicinity of the origin (small k) at values of D close to D_c. As can be seen from Figs. 9c, 11c and 12f, the band structure at $D \sim D_c$ is qualitatively the same for any ratio I/J: there are two weakly dispersed branches with high energy $\sim D$ (purple and yellow curves), one Goldstone mode with linear in k dispersion (red curve), and a blue dispersion curve with visually undetectable type of k-dependence in the vicinity of $k = 0$.

Since the band structure of the SU3-F ceases to change qualitatively at $D > D_c$, then to determine the dispersion of the blue curve at small k we can consider the values of the SIA-parameter from the right neighborhood of D_c. In this case, for the corresponding branches of the spectrum we have analytical expressions (44).

Using these expressions, we obtain the following formula for function $\epsilon_2(k)^2$ (corresponding to the blue branch of the spectrum) up to the fourth degree in absolute value of the dimensionless wave vector $k = \sqrt{k_z^2 + k_x^2}$:

$$\left(\epsilon_2(k)\right)^2 \simeq \rho \frac{J_0^2 S^2}{6} k^2 + \left[2 - \rho\left(3 + \frac{8}{3}\left(\frac{J_0}{D}\right)^2 \frac{D_c}{D} S^2\right)\right] \frac{J_0^2 S^2}{96} k^4, \tag{51}$$

where $\rho = 1 - D_c/D$ is a positive small parameter. It can be seen from the formula (51) that as long as $\rho \neq 0$ (i.e., as long as D is greater than and not equal to D_c), the dependence of $\epsilon_2(k)$ on k is linear: $\epsilon_2(k) \simeq (J_0 S\sqrt{\rho/6})\, k$. But as soon as ρ turns to zero (for $D = D_c$), the spectrum $\epsilon_2(k)$ turns out to be quadratic for small k: $\epsilon_2(k) \simeq (J_0 S/4\sqrt{3})\, k^2$.

Obviously, when D tends to D_c from the left, the spectrum $\epsilon_2(k)$ is modified in a similar way.

11. Concluding remarks

In the present paper, the magnetic and spectral properties of the three-sublattice mixed spin SU(3)-ferrimagnet on triangular lattice at zero temperature have been studied. The magnitude of spins in one (L-) sublattice is $S = 1$, and in the other two, F- and G-sublattices, is $S = 1/2$. As it should be in any ferrimagnet, the exchange interaction between spins from different sublattices is of antiferromagnetic type. The important feature of the system under consideration is due to the single-ion easy plane anisotropy in the spin-1 L-sublattice. This anisotropy can be strong enough to make the SU(3)-ferrimagnet enter the quadrupole phase. As it is known, in this case, three rotation group generators are not enough to describe static and dynamic properties and it is necessary to include extra (in general, all $n^2 - 1$) operators from the $SU(n)$ algebra, where $n = 2S + 1$. It is this circumstance that encouraged us to denote the system in question as the quantum SU(3)-ferrimagnet.

The spectral properties of the SU3-F have been studied within the spin-wave approximation employing Holstein-Primakov representation for spin-1/2 operators from F- and G-sublattices. For spin-1 operators from L-sublattice, due to the comment made above, this representation is incorrect if the constant of the single-ion anisotropy D is not small compared to the exchange integral I. In this regime, a strong quantum fluctuations occur in the L-sublattice. If there is nothing that prevents quantum effects, for instance, an effective field on the anisotropic ion [18], the average spin can be reduced down to zero: $R_L = \langle S_l^z \rangle = 0$. The three-sublattice ferrimagnet considered in this study has the remarkable property that the effective field on the L-sublattice ion, created by antiferromagnetically coupled moments from two isotropic spin-1/2 F- and G-sublattices, is significantly reduced and, therefore, does not prevents the quantum spin reduction on L-sublattice ions.

To correctly account for the SU(3) algebra of operators acting in the L-subsystem Hilbert space, the Hubbard operators representation has been used [47], and bosonization of the Hubbard operators (after the unitary transformation [8,45], diagonalizing the single-ion part of the Hamiltonian) has been carried out according to the recipe suggested in Refs. [7,46].

Numerical calculations of the magnetic structure have given the following picture. At $D = 0$, the magnetic moments of the three sublattices $\mathbf{R}_L$, $\mathbf{R}_F$ and $\mathbf{R}_G$ form a planar structure shown in Fig. 3. The initial (i.e., at $D = 0$) angle θ depends on the ratio of the exchange integrals I and J. At $I < J$ it is less than π, and at $I \geqslant J$ the initial angle $\theta = \pi$. Accordingly, in the first case ($I < J$), the system is in a canted ferrimagnetic phase (with total magnetization $M > 0$) and in the second case ($I \geqslant J$) – in a collinear ferrimagnetic phase when the magnetic moment $\mathbf{R}_L$ is directed along the Oz axis, $\mathbf{R}_F$ and $\mathbf{R}_G$ – against, but the total magnetization $M = 0$, what actually means that this is the first compensation point.

As the SIA-parameter increases, the angle θ decreases, and when the parameter D reaches the critical value $D_c = 2I_0^2/J_0$, the angle θ takes the value of $\pi/2$, and spins in the F- and G-sublattices turns out to be oriented strictly opposite each other and parallel to the Ox axis. At the same time, the L-subsystem enters a singlet non-magnetic state with $R_L = 0$, but with a non-zero quadrupole order parameter Q_2^0 (49). This means that at $D = D_c$ SU3-F enters the quadrupole antiferromagnetic phase.

Dependence of the total magnetization M on the anisotropy parameter D is also determined by the ratio of the exchange integrals I/J. The calculation results for different values of I/J are shown in Fig. 8. The most interesting is the dependence of M on D for $I/J = 1.2$. As shown in Fig. 7a by black curve the total magnetization M turns to zero not only at the boundaries of the interval $[0, D_c]$, but also at two intermediate points and, accordingly, with an increase in D within the specified interval, the value of M changes the sign twice. In this case, four compensation points are actually observed with change in the parameter D: two on the boundaries and two inside the interval $[0, D_c]$. Compensation behavior is interesting both from the experimental point of view and from the technological one. For this reason the SU(3)-ferrimagnet under consideration with the exchange parameter ratio $I \gtrsim J$ can be considered as promising for practical applications.

The relationship $I > J$ for the exchange integrals is also interesting because in this case with an increase in the SIA-parameter all three types of magnetic structure in SU3-F are successively implemented (see Fig. 7a): (1) collinear ferrimagnetic (at $D \in [0, D_*]$); (2) canted ferrimagnetic (at $D \in (D_*, D_c)$); (3) quadrupole antiferromagnetic (at $D \geqslant D_c$).

The spin-wave excitation spectrum of the SU3-F, as calculations have shown, is determined by four branches (Figs. 9, 11 and 12). Two of them (yellow and purple) are associated with excitations in the spin-1 subsystem. One of these two branches (purple) is dispersionless and is always separated by a gap. The second one (yellow) turns to zero at Γ point of the Brillouin zone only at $I \geqslant J$ and $D = 0$. For all other parameters of the model this branch is characterized by a gap, the value of which is larger the larger is the anisotropy parameter D. At $D \to D_c$, the yellow and purple dispersion curves practically merge.

The other two of the four branches of the spin wave spectrum (blue and red in Figs. 9, 11 and 12) are low-energy. The red branch represents the Goldstone mode associated with the rotational (around the Oy axis) symmetry of the Hamiltonian which is always broken in the considered ordered phase.

The blue dispersion curve describes excitations due to rotation of the spins in the F- and G-sublattices about the L-sublattice magnetic moment direction (i.e., about Oz axis). This conclusion is inferred from the analysis of change in the gap Δ_0 in the spectrum described by the blue curve with an increase in the SIA-parameter at the ratio of exchange integrals $I/J > 1$ (Fig. 13). For D less than a certain value D_* the gap Δ_0 is finite, and SU3-F is in collinear ferrimagnetic phase ($\theta = \pi$). As soon as D gets larger than D_*, the F- and G-sublattice magnetization vectors start canting ($\theta < \pi$), and the gap Δ_0 turns to zero. Strictly speaking the Goldstone theorem is not applicable here, because requiring the magnetization canting in the F- and G-sublattices to occur precisely in the zOx plane (and not in any other plane containing the Oz axis), we brake symmetry (with respect to rotation of the vectors $\mathbf{R}_F$ and $\mathbf{R}_G$ about the Oz axis) of not the Hamiltonian (it does not have such a symmetry), but its average value — the energy functional, provided that the vector of L-sublattice average magnetization $\mathbf{R}_L$ is parallel to the Oz axis. Nevertheless, it can be seen from Figs. 12 and 13 that as soon as magnetization canting occurs in the F- and G-sublattices (i.e. the symmetry of the ground state turns out to be lower than that of the energy functional), the blue curve immediately becomes gapless, i.e. behaves like a Goldstone mode.

With regard to the above arguments, it is necessary to exercise some caution, because when making a statement about invariance of the energy of the system with respect to the rotation of the vectors $\mathbf{R}_F$ and $\mathbf{R}_G$ about the direction $\mathbf{R}_L$, it should be remembered that we mean the energy of the system calculated in the spin-wave approximation. Taking into account quantum fluctuations can probably break this invariance.

Another important feature of the blue dispersion curve is related to the modification of its wave vector dependence at the point $D = D_c$: if away from this point the k-dependence of the blue curve is linear, then at the very point $D = D_c$ it turns out to be quadratic.

Note also that the set of parameters $I = J$ and $D = 0$ is the only one at which the three lower branches of spin-wave excitations are gapless (see Fig. 11a), at all other parameters of the model, the number of gapless branches is less than three.

In conclusion we will make one more important general comment. In $SU(3)$-ferrimagnets the need to involve quadrupole degrees of freedom may arise even when the magnitude of the single-ion anisotropy is much smaller than that of exchange interactions, i.e. even in the regime

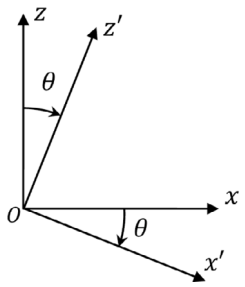

Fig. 14. Two coordinate frames related to each other by rotation about Oy-axis by an angle θ. Note that the axes Oy and Oy' coincide.

of weak anisotropy. Indeed, the condition of not smallness of the SIA means that $D \sim D_c = 2I_0^2/J_0$. But at $I_0 \ll J_0$, this condition can be satisfied even for D much smaller than I_0. Thus for the quantum effects due to SIA to be manifested the parameter D can be small compared to the exchange integral I. This circumstance assigns a special role to the $SU(3)$-ferrimagnets.

CRediT authorship contribution statement

A.S. Martynov: Visualization, Validation, Software, Investigation. **D.M. Dzebisashvili:** Writing – review & editing, Writing – original draft, Supervision, Formal analysis, Conceptualization.

Declaration of competing interest

The authors declare that they have no known competing financial interests or personal relationships that could have appeared to influence the work reported in this paper.

Data availability

No data was used for the research described in the article.

Acknowledgments

The authors thanks professor V.V. Val'kov for original idea of this article, for his continuous interest and enormous contribution to this work. The study was performed within the state assignment of Kirensky Institute of Physics.

Appendix A. SU(2) transformation for spin operators

We want to express the spin operators in one coordinate frame, $Oxyz$, in terms of spin operators in another one, $Ox'y'z'$, obtained by rotating the first frame about Oy-axis (see Fig. 14). For definiteness consider the spin operator S^z which measures the spin projection along Oz-axis in the first coordinate frame. Rotating the operator S^z about Oy-axis by an angle θ we get a spin operator $S^{z'}$ measuring spin projection along Oz'-axis. Mathematically, this rotation corresponds to the unitary transformation: $S^{z'} = e^{-i\theta S^y} S^z e^{i\theta S^y}$ (see, for example, [48]). Given that $S^{y'} \equiv S^y$ it can be rewritten as

$$\begin{aligned} S^z &= e^{i\theta S^y} S^{z'} e^{-i\theta S^y} = e^{i\theta S^{y'}} S^{z'} e^{-i\theta S^{y'}} \\ &= S^{z'} \cos\theta - S^{x'} \sin\theta, \end{aligned}$$

which, after replacing, for simplicity, $z' \to z$ and $x' \to x$ is the third equality in (5). The first equality in (5) is obtained in a similar way.

Appendix B. SU(3) transformations for hubbard and spin operators

Let us define a generator of the $SU(N)$ algebra as $\Gamma_{nm} = X^{nm} - X^{mn}$ with n and m ($n \neq m$) being the numbers of two certain states in the Hilbert space under consideration. Following Ref. [45], write down the unitary operator (28) for one particular site as follows (site index is omitted):

$$\begin{aligned} &U_{nm}(\alpha) = \exp\left\{\alpha \Gamma_{nm}\right\} = \\ &= 1 + (\cos\alpha - 1)\left(X^{nn} + X^{mm}\right) + \sin\alpha\ \Gamma_{nm}. \end{aligned} \tag{B.1}$$

The new Hubbard operators $X^{\tilde{r}\tilde{s}} = |\tilde{r}\rangle\langle\tilde{s}|$, defined in terms the new states

$$|\tilde{r}\rangle = U_{nm}(-\alpha)|r\rangle, \tag{B.2}$$

can be expressed via the initial Hubbard operators $X^{rs} = |r\rangle\langle s|$ by means of the unitary transformation

$$X^{\tilde{r}\tilde{s}} = U_{nm}(-\alpha) X^{rs} U^{+}_{nm}(-\alpha). \tag{B.3}$$

Since by definition (B.1) the operator $U_{nm}(\alpha)$ commutes with the generator Γ_{nm}, we have

$$\Gamma_{\tilde{n}\tilde{m}} = U_{nm}(-\alpha)\Gamma_{nm}U^{+}_{nm}(-\alpha) = \Gamma_{nm}, \tag{B.4}$$

Inverting Eq. (B.3), i.e. expressing initial operator X^{rs} via the new one $X^{\tilde{r}\tilde{s}}$, and accounting for the equality $U_{\tilde{n}\tilde{m}}(\alpha) = U_{nm}(\alpha)$, following from Eq. (B.4), we get

$$\begin{aligned} X^{rs} &= U_{nm}(\alpha) X^{\tilde{r}\tilde{s}} U^{+}_{nm}(\alpha) \\ &= U_{\tilde{n}\tilde{m}}(\alpha) X^{\tilde{r}\tilde{s}} U^{+}_{\tilde{n}\tilde{m}}(\alpha), \end{aligned} \tag{B.5}$$

which is the desired expression.

The right hand side of (B.5) can be evaluated explicitly for particular r and s:

$$\begin{aligned} X^{nn} &= \cos^2\alpha\, X^{\tilde{n}\tilde{n}} + \sin^2\alpha\, X^{\tilde{m}\tilde{m}} \\ &\quad - \frac{1}{2}\sin 2\alpha \left(X^{\tilde{n}\tilde{m}} + X^{\tilde{m}\tilde{n}}\right), \\ X^{mm} &= \cos^2\alpha\, X^{\tilde{m}\tilde{m}} + \sin^2\alpha\, X^{\tilde{n}\tilde{n}} \\ &\quad + \frac{1}{2}\sin 2\alpha \left(X^{\tilde{n}\tilde{m}} + X^{\tilde{m}\tilde{n}}\right), \\ X^{nm} &= \cos^2\alpha\, X^{\tilde{n}\tilde{m}} - \sin^2\alpha\, X^{\tilde{m}\tilde{n}} \\ &\quad + \frac{1}{2}\sin 2\alpha \left(X^{\tilde{n}\tilde{n}} - X^{\tilde{m}\tilde{m}}\right), \\ X^{mn} &= \cos^2\alpha\, X^{\tilde{m}\tilde{n}} - \sin^2\alpha\, X^{\tilde{n}\tilde{m}} \\ &\quad + \frac{1}{2}\sin 2\alpha \left(X^{\tilde{n}\tilde{n}} - X^{\tilde{m}\tilde{m}}\right), \\ X^{np} &= \cos\alpha\, X^{\tilde{n}\tilde{p}} - \sin\alpha\, X^{\tilde{m}\tilde{p}}, \\ X^{pn} &= \cos\alpha\, X^{\tilde{p}\tilde{n}} - \sin\alpha\, X^{\tilde{p}\tilde{m}}, \\ X^{pm} &= \cos\alpha\, X^{\tilde{p}\tilde{m}} + \sin\alpha\, X^{\tilde{p}\tilde{n}}, \\ X^{mp} &= \cos\alpha\, X^{\tilde{m}\tilde{p}} + \sin\alpha\, X^{\tilde{n}\tilde{p}}, \\ X^{pq} &= X^{\tilde{p}\tilde{q}}, \qquad (p,q \neq n,m). \end{aligned} \tag{B.6}$$

In our case the spin $S = 1$ and the indices n and m take the values $1, 0, -1$. Using relevant expressions from (B.6) in the Eq. (21) the transformation laws for spin operators can be easily obtained

$$\begin{aligned} S^x(\alpha) &= \frac{1}{\sqrt{2}}(\cos\alpha + \sin\alpha)\left(X^{\tilde{1},\tilde{0}} + X^{\tilde{0},\tilde{1}}\right) \\ &\quad + \frac{1}{\sqrt{2}}(\cos\alpha - \sin\alpha)\left(X^{-\tilde{1},\tilde{0}} + X^{\tilde{0},-\tilde{1}}\right), \\ S^y(\alpha) &= \frac{i}{\sqrt{2}}(\sin\alpha - \cos\alpha)\left(X^{\tilde{1},\tilde{0}} - X^{\tilde{0},\tilde{1}}\right) \\ &\quad + \frac{i}{\sqrt{2}}(\cos\alpha + \sin\alpha)\left(X^{-\tilde{1},\tilde{0}} - X^{\tilde{0},-\tilde{1}}\right), \\ S^z(\alpha) &= \cos 2\alpha \left(X^{\tilde{1},\tilde{1}} - X^{-\tilde{1},-\tilde{1}}\right) \\ &\quad - \sin 2\alpha \left(X^{\tilde{1},-\tilde{1}} + X^{-\tilde{1},\tilde{1}}\right). \end{aligned} \tag{B.7}$$

References

[1] L. Landau, E. Lifshits, On the theory of the dispersion of magnetic permeability in ferromagnetic bodies, Phys. Z. Sow. 8 (1935) 153.

[2] H.H. Chen, P.M. Levy, Quadrupole phase transitions in magnetic solids, Phys. Rev. Lett. 27 (1971) 1383.

[3] V.M. Matveev, Quantum quadrupolar magnetism and phase transitions in the presence of biquadratic exchange, Zh. Eksp. Teor. Fiz. 65 (1973) 1626.

[4] M.P. Kashchenko, N.F. Balakhonov, L.V. Kurbatov, Spin waves in an Heisenberg ferromagnetic substance with single-ion anisotropy, Zh. Eksp. Tear. Fiz. 64 (1973) 391.

[5] F.P. Onufrieva, Exact solution of the one-ion problem for a magnet with one-ion anisotropy in a field of arbitrary direction, Zh. Eksp. Teor. Fiz. 80 (1981) 2372.

[6] A.F. Andreev, I.A. Grishchuk, Spin nematics, Zh. Eksp. Teor. Fiz. 87 (1984) 467.

[7] F.P. Onufrieva, Low-temperature properties of spin systems with tensor order parameters, Zh. Eksp. Teor. Fiz. 62 (1985) 1311.

[8] V.M. Loktev, V.S. Ostrovskii, Quantum theory of uniaxial ferromagnetic in transverse magnetic field, Ukr. J. Phys. 23 (1978) 1717.

[9] N. Papanicolaou, Unusual phases in quantum spin-1 systems, Nuclear Phys. B 305 (1988) 367.

[10] A.V. Chubukov, Fluctuations in spin nematics, J. Phys.: Condens. Matter 2 (1990) 1593.

[11] V.V. Val'kov, T.A. Val'kova, Application of an indefinite metric to go over to a Bose description of SU(3) Hamiltonians: The excitation spectrum of spin nematics, Zh. Eksp. Teor. Fiz. 99 (1991) 1881.

[12] Yu.A. Fridman, O.A. Kosmachev, Ph.N. Klevets, Spin nematic and orthogonal nematic states in $S = 1$ non-Heisenberg magnet, JMMM 325 (2013) 125.

[13] B. Barbara, Y. Imry, G. Sawatzky, P.C.E. Stamp, Quantum magnetism, in: NATO Science for Peace and Security Series B: Physics and Biophysics, Springer Dordrecht, 2008, p. 249.

[14] A. Auerbach, Interacting Electrons and Quantum Magnetism, Springer-Verlag, New York, Inc., 1994, p. 255.

[15] A.I. Smirnov, Magnetic resonance of spinons in quantum magnets, Phys.-Usp. 59 (2016) 564.

[16] C. Lacroix, P. Mendels, F. Mila, Introduction to frustrated magnetism, in: Springer Series in Solid-State Sciences, 2011, p. 682.

[17] B.A. Ivanov, A.K. Kolezhuk, Effective field theory for the $S = 1$ quantum nematic, Phys. Rev. B 68 (2003) 052401.

[18] Y.A. Fridman, O.A. Kosmachev, Quantum effects in an anisotropic ferrimagnet, Phys. Solid State 51 (2009) 1167.

[19] A. Lauchli, F. Mila, K. Penc, Quadrupolar phases of the $S = 1$ bilinear-biquadratic Heisenberg model on the triangular lattice, Phys. Rev. Lett. 97 (2006) 087205.

[20] V.V. Val'kov, M.S. Shustin, Quantum theory of strongly anisotropic two- and four-sublattice single-chain magnets, J. Low Temp. Phys. 185 (2016) 564.

[21] M. Blume, Y.Y. Hsieh, Biquadratic exchange and quadrupolar ordering, J. Appl. Phys. 40 (1969) 1249.

[22] J. Chen, S. Hu, L. Pan, X. Wang, Nonuniform quadrupolar orders in the spin-3/2 generalized Heisenberg chain, 2023, arXiv:2311.08099v1 [cond-mat.str-el].

[23] A.V. Chubukov, K.I. Ivanova, P.Ch. Ivanov, E.R. Korutcheva, Quantum ferrimagnets, J. Phys.: Condens. Matter 3 (1991) 2665.

[24] F. Michaud, F. Mila, Phase diagram of the spin-1 Heisenberg model with three-site interactions on the square lattice, Phys. Rev. B 88 (2013) 094435.

[25] I. Affleck, Large-n limit of SU(N) quantum spin chains, Phys. Rev. Lett. 54 (1985) 966.

[26] D.P. Arovas, A. Auerbach, Functional integral theories of low-dimensional quantum Heisenberg models, Phys. Rev. B 38 (1988) 316.

[27] N. Read, S. Sachdev, Some features of the phase diagram of the square lattice SU(N) antiferromagnet, Nuclear Phys. B 316 (1989) 609.

[28] K.S.D. Beach, SU(N) Heisenberg model on the square lattice: A continuous-N quantum Monte Carlo study, Phys. Rev. B 80 (2009) 184401.

[29] J. Schwab, F.P. Toldin, F.F. Assaad, Phase diagram of the SU(N) antiferromagnet of spin S on a square lattice, Phys. Rev. B 108 (2023) 115151.

[30] H.F. Verona de Resende, F.C. SaBarreto, J.A. Plascak, Renormalization group treatment of the mixed-spin system in d-dimensional lattices, Physica A 149 (1988) 606.

[31] G.M. Zhang, C.Z. Yang, Monte Carlo study of the two-dimensional quadratic Ising ferromagnet with spins $S = 1/2$ and $S = 1$ and with crystal-field interactions, Phys. Rev. B 48 (1993) 9452.

[32] A. Bobak, M. Jurcisin, A discussion of critical behaviour in a mixed-spin Ising model, Physica A 240 (1997) 647.

[33] G.M. Buendia, M.A. Novotny, Numerical study of a mixed Ising ferrimagnetic system, J. Phys.: Condens. Matter 9 (1997) 5951.

[34] M. Godoy, W. Figueiredo, Competing dynamics in the mixed-spin Ising model with crystal-feld interaction, Physica A 339 (2004) 392.

[35] T. Iwashita, N. Uryu, The curie temperature of the two-dimensional quadratic Ising ferromagnet with mixed spins of $S = 1/2$ and S=1, J. Phys. Soc. Japan 53 (1984) 721.

[36] J. Oitmaa, Ferrimagnetism and the existence of compensation points in layered mixed spin (1/2, 1) Ising models, Phys. Rev. B 72 (2005) 224404.

[37] J. Oitmaa, I.G. Enting, A series study of a mixed-spin $S = (1/2, 1)$ ferrimagnetic Ising model, J. Phys.: Condens. Matter 18 (2006) 10931.

[38] W. Selke, J. Oitmaa, Monte Carlo study of mixed-spin $S = (1/2, 1)$ Ising ferrimagnets, J. Phys.: Condens. Matter 22 (2010) 076004.

[39] M. Zukovic, A. Bobak, Frustrated mixed spin-1/2 and spin-1 Ising ferrimagnets on a triangular lattice, Phys. Rev. E 91 (2015) 052138.

[40] M. Zukovic, A. Bobak, Mixed spin-1/2 and spin-1 Ising ferromagnets on a triangular lattice, Physica A 436 (2015) 509.

[41] E.S. de Santana, A.S. de Arruda, M. Godoy, Random-anisotropy mixed-spin Ising on a triangular lattice, Condens. Matter Phys. 26 (2023) 23601.

[42] Yu.A. Fridman, D.V. Spirin, Spin waves in two-dimensional ferromagnet with large easy-plane anisotropy, J. Magn. Magn. Mater. 253 (2002) 111.

[43] O.A. Kosmachev, Ya.Yu. Matyunina, Yu.A. Fridman, J. Exp. Theor. Phys. 135 (2022) 354.

[44] L.D. Landau, E.M. Lifshitz, Quantum Mechanics: Non-Relativistic Theory, vol. 3, Elsevier, 2013.

[45] V.V. Val'kov, Unitary transformations of the group $U(N)$ and diagonalization of multilevel Hamiltonians, Theoret. Math. Phys. 76 (1988) 766.

[46] V.V. Val'kov, T.A. Val'kova, Anomalies in the quantum excitation spectrum of a magnetic material with a strong quasiparticle interaction, JETP Lett. 52 (1990) 1179.

[47] J. Hubbard, Electron correlations in narrow energy bands III. An improved solutions, Proc. Roy. Soc. A 281 (1964) 401.

[48] C. Cohen-Tannoudji, B. Diu, F. Laloe, Quantum Mechanics, vol. 1, Wiley-VCH, 2019, p. 944.